Biophysical Journal
Article

Biophysical Society

Environmental conditions define the energetics of bacterial dormancy and its antibiotic susceptibility

Leonardo Mancini[1] and Teuta Pilizota[1,*]
[1]School of Biological Sciences, Centre for Synthetic and Systems Biology, University of Edinburgh, Edinburgh, United Kingdom

ABSTRACT Bacterial cells that stop growing but maintain viability and the capability to regrow are termed dormant and have been shown to transiently tolerate high concentrations of antimicrobials. Links between tolerance and cellular energetics as a possible explanation for the tolerance, have been investigated and have produced mixed and seemingly contradictory results. Because dormancy merely indicates growth arrest, which can be induced by various stimuli, we hypothesize that dormant cells may exist in a range of energetic states that depend on the environment. To energetically characterize different dormancies, we first induce them in a way that results in dormant populations and subsequently measure both of their main energy sources, the proton motive force magnitude and the concentration of ATP. We find that different types of dormancy exhibit characteristic energetic profiles that vary in level and dynamics. The energetic makeup was associated with survival to some antibiotics but not others. Our findings portray dormancy as a state that is rich in phenotypes with various stress survival capabilities. Because environmental conditions outside of the lab often halt or limit microbial growth, a typologization of dormant states may yield relevant insights on the survival and evolutionary strategies of these organisms.

SIGNIFICANCE The surge of antibiotic resistance calls for a better understanding of bacterial survival strategies. Dormant bacteria are exceptionally good at surviving treatments. Several studies have explored the association between dormancy and energetics, producing contradicting results. Here we reconcile these contradictions by showing that there is no one size fits all for the energetics of dormancy. We show at the single cell level that depending on the factors that lead and kept them into dormancy, cells' proton motive force, ATP concentration and internal pH can vary from growth-like to low. We then show that the energy profiles associated with given dormancies influence survival under certain antibiotics and not others, supporting the notion that dormancy can produce different treatment-relevant phenotypes.

INTRODUCTION

The global surge of antibiotic resistance in both clinical and environmental isolates calls for a better understanding of bacterial survival strategies (1). Bacteria causing infections that are hard to treat are commonly characterized as resistant, persistent, or tolerant, depending on whether they owe their survival to genotypical or phenotypical changes and/or their death rate under antibiotic treatment (2,3). Regardless of the genotype, temporary growth cessation is often linked to survival, and dormancy is regarded as the silver bullet against a wide spectrum of antibiotics (4), as it enables infection recalcitrance (5) and facilitates the evolution of higher levels of resistance (6–9).

Microbes can enter dormancy for a number of reasons, but the mechanisms by which dormancy is attained and maintained and how it leads to survival are multifaceted and often poorly understood (10,11). Consequently, even the definition of dormancy can vary between different reports. Despite this, it is attractive to investigate if there is a dominant feature of dormancy that underpins much of its protective effects. One of the leading hypotheses is that dormancy reduces the activity of antibiotic targets (4), but other mechanisms have been proposed. For example, several studies have attempted to establish a link between cellular energy (ATP in particular) and survival capabilities of dormant cells, with results that are seemingly contradictory (12–21). On one hand, stationary *Staphylococcus aureus*, arsenate-poisoned, and HokB toxin-expressing *Escherichia coli* were found to have reduced levels of ATP and high tolerance to ciprofloxacin, ampicillin, and

Submitted February 2, 2023, and accepted for publication June 30, 2023.

*Correspondence: teuta.pilizota@ed.ac.uk

Leonardo Mancini's present address is Department of Physics, Cavendish Laboratory, University of Cambridge, Cambridge, United Kingdom.

Editor: Ido Golding.

https://doi.org/10.1016/j.bpj.2023.06.023

ofloxacin, respectively (12,13,19). Similarly, *E. coli* cells with high ATP levels were found more susceptible to β-lactams and fluoroquinolones (17), those with low ATP levels less susceptible to the β-lactam ampicillin (20), and cells with low respiration rates were found to deal better with several bactericidal antibiotics (18). On the other hand, *Salmonella enterica* cells with reduced ATP levels, due to deletion of the *atp* operon, were more susceptible to ciprofloxacin (14), and those with increased levels of ATP were less susceptible to antibiotics (21). Furthermore, ATP concentration was not low in ampicillin-tolerant stationary phase and amino-acid starved *E. coli* (15,16). These apparently contradictory results arise mostly from studies that assume all dormant states would be equivalent from an energetic and drug susceptibility perspective, despite being attained in different ways. Relaxing this assumption, that is, demonstrating that different dormant states come with different energy profiles (including different temporal profiles) and drug susceptibilities, could potentially reconcile them, furthering the notion that the protective effects of dormancy cannot be oversimplified (22).

A systematic mapping of the energetic profiles of different types of dormant cells would not only reconcile the seemingly contradictory results mentioned above by showing various possible energetic states, but it would also have relevant repercussions on treatment design. However, this has thus far not been possible, primarily because dormancy has been studied mostly in spontaneously occurring persistent cells from heterogeneous populations. These cells are low in numbers, and their study is limited to high-throughput single-cell techniques (23,24). Also as a consequence of this, most previous measurements of energy levels in dormant cells focus on just one of the two main energy sources in microbes, the ATP molecule. The other one, the so called proton motive force (PMF), has not been easily accessible until recently (25–27), and the technique that we showed can estimate it precisely, dynamically, and with high temporal resolution is still low in throughput (27). The PMF is the electrochemical gradient of protons across the cytoplasmic membrane, and it plays a fundamental role in cell physiology, powering transport across the plasma membrane (28–31), including those mediated by multidrug efflux pumps (32), fueling the production of ATP via the F_1 F_o ATP synthase, as well as regulating pH homeostasis (33) and is thus very likely important during antibiotic challenges.

To initiate a typologization of dormant states based on their energy profiles, we first established a protocol that ensured we could work with a large number of dormant cells in a given environmental condition. Then, we systematically mapped at the single-cell level the energetics of cells that entered dormancy in response to different external stimuli. We sought to draw a more extensive picture of the main cellular energy sources and thus focused on PMF, its pH component, and the ATP concentration. Our results show that the energetic states of cells that entered dormancy due to different extracellular conditions are not equivalent and can range from growth-like to markedly reduced. In addition, we found that the energy profile and levels associated with a given dormancy-inducing stimulus influence the survival to certain antibiotics and not others. For the former, the importance of energetics could, to a first-order approximation, be explained with the role of PMF/ATP on characteristic antibiotic accumulation/efflux. The survival of dormant cells, therefore, does not only depend on the reduced activity of antibiotic targets, but other antibiotic-specific mechanisms can come into play. These could be interesting targets for treatment. Our work portrays dormancy as a phenotypically complex state, a notion that we expect applies to similar states in other organisms and that shows that knowledge of the environmental conditions present at the infection site is important for the design of accurate treatment strategies.

MATERIALS AND METHODS

Bacterial strains

Experiments were carried out using *E. coli* EK01 and EK07 strains (27). The strains have an MG1655 background with the FliC-sticky mutation (EK01), which allows polystyrene beads to stick to bacterial flagella, and the pH sensor pHluorin gene (EK07), both incorporated into the chromosome. For ATP concentration measurements, the EK01 strain was transformed with the plasmid pTP20-QUEEN7* that expresses the QUEEN 7μM* sensor downstream of a strong constitutive promoter, as shown in Fig. S8. As in (34), the plasmid was constructed by PCR amplification of the backbone from plasmid pWR20 (35) and the sequence containing Q7*. Later steps included purification of the PCR products followed by restriction with the restriction enzymes AvrII and NotI (NEB, UK) and ligation with the T4 DNA ligase (Promega, UK). Chemically competent cells were transformed with the ligation mixes, and resulting strains were confirmed with colony PCR and sequencing. A map of the plasmid pTP20-QUEEN7* and the primers are given in supporting material (Fig. S8 and Table S1). Strains used in this work are listed in Table S2.

Bacterial growth conditions

For measurements of cellular energetics, cells were grown in M63 (36) (13.6 g/L KH_2 PO_4, 0.5 mg/L $FeSO_4 \cdot 7$ H_2O, 0.5 g/L $MgSO_4 \cdot 7$ H_2O, 1.27 mg/L thiamine, 2.64 g/L $(NH_4)2$ SO_4, and 0.5% w/v glucose, final pH: 7.2) to balanced growth at 37°C with shaking at 220 rpm. Balanced growth was achieved by inoculating single colonies into LB medium (0.5% yeast extract, 1% Bacto tryptone, 0.5% NaCl) for 3 to 4 h. Cells from such culture were grown to optical density (OD) 0.3–0.4 in M63 from a starting dilution of 10^{-7}. In the case of the EK01-pTP20-Q7* strain, 50 μg/mL of kanamycin was added to the medium.

OD readings in the presence of various concentrations of indole, bacteriostatic antibiotics, or in carbon- or nitrogen-deprived medium were obtained in a Spectrostar Omega microplate reader (BMG, Germany) using a flat-bottom 96-well plate that was covered with a lid during the experiments (Costar, UK). Cells grown to balanced growth were collected at OD 0.3–0.4 and transferred to the dormancy-inducing medium at a 1:1 dilution by centrifuging them at 8000 *g* for 2 min and washing them twice in the new medium. This ensured the OD at the beginning of the measurements was within the microplate reader's sensitivity range ($\sim$ 0.2). Empty wells adjacent to the samples were filled with water to minimize evaporation. Plates were grown at 37°C with 700 rpm shaking (double orbital mode) for 5 or 24 h with readings taken every 12 min.

For fluorescence intensity comparisons (Figs. 3 *A* and S4 *A*) and for in vitro studies on cell lysates, we inoculated single colonies in LB medium with 50 μg/mL of kanamycin and grew them overnight at 37°C with shaking at 220 rpm. We then inoculated RDM with glucose (37,38) with 50 μg/mL of kanamycin with the overnight culture at 1:1000 dilution and grew it at 37°C with shaking at 220 rpm to OD 0.3–0.5.

Fluorescence microscopy and motor speed measurements

Imaging was carried out in a custom-built microscope with a 100× oil immersion objective lens (Nikon, Japan) (27,39). Illumination for the cells expressing pHluorin sensor was provided by a neutral white LED with the filter ET470/40x (Chroma Technology, USA) and a UV LED (Cairn, UK). Cells expressing the Q7* sensor were illuminated with the same UV LED and a 488-nm laser (Vortran Laser Technology, USA). Images were taken with an iXon Ultra 897 EMCCD camera (Andor, UK) (39,40). For both sensors, emission was measured with the ET525/40m filter (Chroma Technology, USA). In the case of pHluorin, images were taken at 1.5-min intervals, exposure time was 50 ms, and Andor camera gain was 100. Q7* was instead imaged only once per field of view with the same exposure time but with 50 Andor camera gain. Intensity comparisons were also carried out at 50-ms exposure time and 50 Andor camera gain and kept constant across different sensors. Cells were imaged in a custom-built flow cell ((34)) and attached to the coverslip surface as before (34). Briefly, 0.1% Poly-L-Lysine (Sigma, UK) was flushed through the flow cell and washed with 3–5 mL of growth medium after 10 s. Cells' flagellar filaments were sheared as before (27,34,39) by passing them through two syringes with narrow-gauge needles (26G) connected by plastic tubing. 200 μL of cells was delivered to the flow cell and allowed to attach for 10 min, after which the unattached cells were removed with 1 mL of growth medium. Polystyrene particles (beads) with a diameter of 0.5 μm (Polysciences, USA), were then delivered into the flow cell and allowed to attach to the filament stubs. After 10 min, unattached beads were removed with 1–2 mL of growth medium. Measurements and the whole preparation were performed at 37°C. During measurements, fresh, prewarmed medium was constantly delivered with a peristaltic pump (Fusion 400, Chemyx, USA) using a 100 μL/min flow rate. Cells grow attached to the Poly-L-Lysine surface with expected growth rates (given the medium), as previously reported (41). We note that short time intervals (up to a maximum of 10 min) can sometimes be necessary to find a spinner. During this period, cells are kept in growth medium with no flow, as for these experiments, starting the flow starts the dormancy. This can sometimes lead to small waste accumulations or oxygen depletion visible in the pH traces (this pH drop of 0.1–0.2 observed in Fig. 2 *A* corresponds to 6–12 mV only). Motor speed measurements are carried out at a frequency of 10 kHz (passed through antialiasing filters before recording). Sample sizes for pH and ATP measurements were selected so that the margin of error and 95% confidence is 5% or less. PMF measurements are single-motor, single-cell experiments, so one obtains only one measurement in a 30-min window and for one slide preparation. This was taken into account when determining the sample size, which was selected to achieve the margin of error and 95% confidence around 10%.

QUEEN sensors characterization from lysates

To characterize the sensors in their original conformation while maintaining conditions as similar as possible to the in vivo environment, we performed spectroscopic and microscopic assays on cell lysates. Cells grown in RDM were harvested via centrifugation at 11,000 *g* at 4°C for 30 min. Supernatant was discarded and cells resuspended in ice-cold QUEEN buffer (50 mM HEPES, 200 mM KCl, 1 mM $MgCl_2$, 0.05% Triton X-100, protease inhibitor cocktail (Sigma, GB), pH adjusted to 7.7) (42). 100 μg/ml of lysozyme was added to the cell suspension and incubated for 15 min at room temperature (21°C). Cells were disrupted with a Soniprep 150 sonicator (MSE, UK) with four cycles of 30 s on and 30 s off, making sure that no foam was produced. During sonication, the tube containing the sample was kept in ice-cold water to limit protein damage. The lysates were then filtered with a 0.22-μm filter to remove intact cells and large debris. Solutions with different concentrations of Mg-ATP (Sigma, UK) in QUEEN buffer were mixed with QUEEN lysate maintaining a constant ratio between the two (9:1) in order to maintain a constant protein concentration.

Samples for imaging were prepared in tunnel slides (39) by flushing in sequence: 10 μL 0.1% Poly-L-Lysine (Sigma, UK), 100 μL QUEEN buffer wash, 10 μL of a 1-μm polystyrene bead solution (Polysciences, USA), 100 μL QUEEN buffer wash, and 10 μL of QUEEN lysate and ATP solution. No incubation was needed between the different steps. The slides were then sealed with CoverGrip sealant (Biotium, US). Three distant (at least three fields of view apart) fields of view were imaged with epifluorescence microscopy

from each slide, and the imaging plane was chosen by focusing on the polystyrene beads.

Fluorescence spectra of QUEEN sensors were obtained with an SPEX Fluoromax 3 spectrometer (Horiba, JP). Excitation was scanned from 370 to 500 nm at 513-nm emission with a slit size of 3 nm. The temperature of the sample holder was controlled via a circulating water bath, and readings were taken after letting the temperature of the sample reach equilibrium with that of the sample holder (24°C), i.e., after at least 5 min.

MIC estimation

MIC was estimated on EK07 cells grown to balanced growth. Aliquots of cultures in balanced growth were diluted 1:100 into prewarmed M63 medium (final OD 0.002–0.004) with different concentrations of ciprofloxacin (2, 4, 8, 16, 32, 64, 128, 256 ng/mL) or kanamycin (2, 4, 8, 16, 32, 64, 128, 256 μg/ml). Cell suspensions were then transferred into a prewarmed 96-well plate, incubated for 24 h, and imaged (Fig. S8).

CFU counting

For colony forming units (CFUs) counting, cells were grown to balanced growth, harvested via centrifugation at 8000 *g* for 5 min, and washed twice in the various dormancy-inducing conditions or fresh M63. Cultures were then incubated at 37°C with 220 rpm shaking (the same conditions in which they had been grown). From this point onward, the protocol varies slightly depending on whether we are trying to estimate survival to dormancy-inducing conditions (Fig. 1 *B*) or to the combination of dormancy-inducing conditions and antibiotic treatments (Fig. 4).

For estimating the number of survivors to our dormancy-inducing conditions (Fig. 1 *B*), aliquots of the cultures were taken after 60, 120, 180, and 240 min (Fig. 4 *A*), pelleted at 8000 *g* for 2 min and washed twice in fresh M63 medium. Samples were then serially diluted with a 1:9 ratio in fresh M63 and 10 μL of each dilution spotted on rectangular petri dishes (Thermo Fisher Scientific, UK) containing LB agar. The petri dishes were next tilted to let the liquid spread across the plate as in (43), incubated for 24 h at 37°C, and colonies counted.

For estimating survival to antibiotics (Fig. 4), cells were left in the dormancy-inducing conditions for 30 min. Once dormancy had been established, antibiotics at 5x the MIC (16 ng/mL for ciprofloxacin and 8 μg/ml for kanamycin (Fig. S8)) were added to the cultures. Aliquots of the cultures were taken after 30, 120, 180, and 240 min and plated as explained above (Fig. 4 *A*).

Experiments were carried out in biological triplicates.

Data analysis

Motor speed traces

Raw traces of the x and y position of the bead attached to the filament stub were analyzed by a moving-window discrete Fourier transform in LabView as in (39). From the obtained motor speed traces DC frequency (50 Hz) was removed, speeds lower than 5 Hz ignored, and subsequently a median filter (window size 31) was applied (27,34). We use a chemotactic wild-type strain for which the flagellar motor can change rotational direction, which appears as a negative speed after application of the moving-window Fourier transform. For the purpose of the PMF measurements, these short intervals can be disregarded, and we only show the speed values above 0 Hz as in (34). Because of our flow slide design (34), media switches during treatments happen 2 to 4 min from the start of the recordings. To account for this variability, traces of cells exposed to carbon starvation were aligned taking as a reference an arbitrary motor speed value of 150 Hz, which in our conditions is a good indicator of the timing of bacterial flagellar motor speed drop. For all traces in Fig. 2 *C*, PMF values are normalized to the initial PMF calculated as the average of the first 60 s of the trace.

Fluorescence images

The image analysis was carried out with a custom written PYTHON script. Fluorescence images were initially inspected for any unevenness in the epifluorescence illumination (i.e., in the field of view) by assaying background gray values using the straight line tool of ImageJ (44). To

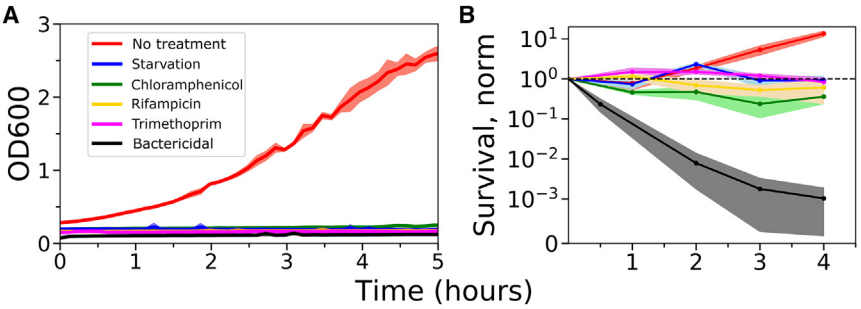

FIGURE 1 Individuation of different dormancies by monitoring cell growth and viability. (*A*) Addition of 200 μg/mL of chloramphenicol, 16 μg/mL rifampicin, 0.2 μg/mL trimethoprim, or removal of the carbon source sharply arrest growth of previously exponentially growing cells. The shaded area shows the standard deviation of three replicates, and experiments were performed in a plate reader. (*B*) Cell viability under candidate dormancies identified in an assay by counting colony forming units (CFUs). The shaded areas show the standard error of three independent replicates. Treatment with 5x MIC ciprofloxacin, a bactericidal antibiotic, and untreated cells are given as controls. The dashed line indicates constant cell number. To see this figure in color, go online.

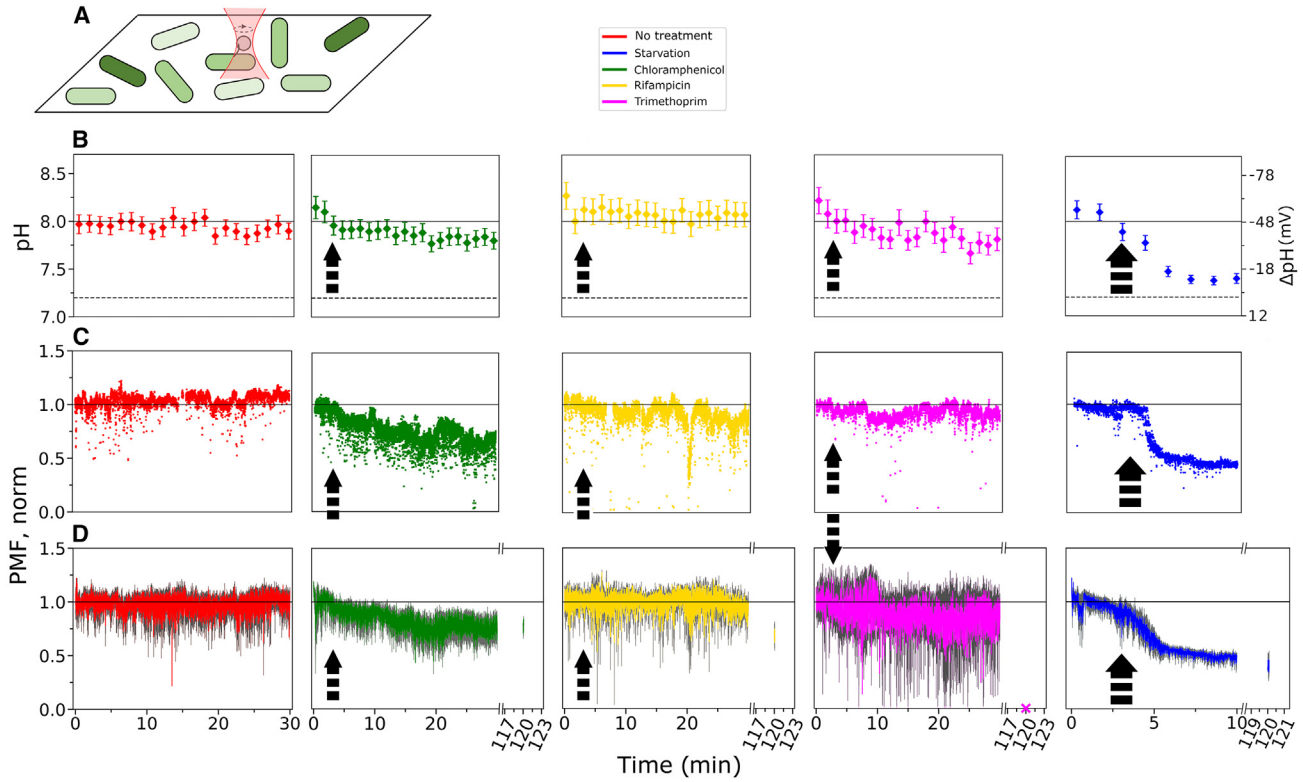

FIGURE 2 Different dormancies are not energetically equivalent. (*A*) Cartoon of a typical field of view in which the flagellar motor speed of a cell is measured simultaneously as its cytoplasmic pH. The pH of all of the neighboring cells in the field of view is also measured. (*B*) Average cytoplasmic pH and Δ pH for cells in growth medium (*M63 with glucose shown in red as a negative control*), with 200 μg chloramphenicol (*green*), 16 μg rifampicin (*yellow*), 0.2 μg trimethoprim (*fuchsia*), or medium deprived of the carbon source (*blue*). Fresh media is continuously supplied to the cells during treatment, and error bars are standard errors. Average values for each time point were obtained from 8 to 10 experiments for a total of 494 cells in M63 with glucose (media), 605 cells in the media with chloramphenicol, 796 cells in the media with rifampicin, 593 cells in the media with trimethoprim, and 594 cells in media with no glucose. With the chosen sample size and 0.95% confidence, we obtain a margin of error of 0.2 points (2.5%) of pH or lower. Due to our flow cell design (34), the switch between growth medium used during slide preparation and dormancy-inducing medium occurs 2 to 4 min (*black arrow, where the width of the arrow indicates the duration of the interval*) from the beginning of the recording. The dashed line indicates the pH of the medium, which is 7.2. The solid black line indicates pH 8. (*C*) Example single-cell, normalized PMF measurements from individual motor speed traces, each in one of the five conditions shown in (*B*). (*D*) Average normalized PMF of 10 cells in each condition. Standard errors are given in gray. The margin of error at 95% is 0.13 (13%) points of normalized PMF or lower. In the case of carbon starvation and chloramphenicol and rifampicin treatment, we also assayed the PMF after 2 h incubation on three, 24, and six cells, respectively. It was not possible to find spinning motors after 2 h in the trimethoprim condition, which could indicate that the PMF may have been lost; we indicate this with a cross. To adjust for the variable arrival time of the treatment to the field of view (after 2–4 min), the 10 PMF traces of the carbon starvation condition (*blue*) were aligned as explained in materials and methods. To see this figure in color, go online.

individuate the cells, objects with high gray values were discerned from the background by applying a global threshold via Otsu's method (45) and labeled. All found objects were inspected for size and aspect ratio so that anything smaller than 8 μm^2 or bigger than 56 μm^2 or with an aspect ratio below 1.7 were excluded. The criteria were set based on the average size, length, and width of cells in our growth condition (balanced exponential growth at the growth rate of 0.7 h^{-1}) and allow us to discard labels that are not correctly segmented and small artifacts. Total cells' intensity values were obtained by summing up and averaging pixel intensities of selected objects.

ATP calibration curves

The sensitivity range of the Q7* protein is independent from imaging conditions and settings. Differences in the optical setup that can alter light intensity, even those arising from small changes in the alignment of the optics, will however change the absolute value of the ATP to 395/488 nm relationship. Calibrations therefore need to be performed periodically (or after any known changes in optics). For comparison, in Fig. 3 *B*, we eliminated the variability between calibrations performed in different days by rescaling the values to the range of the curve used to calculate ATP concentrations in vivo in Fig. 3 *D*. We used the following formula: $(Max_{old} - Min_{old}) \frac{Value - Min_{new}}{Max_{new} - Min_{new}} + Min_{old}$.

Plate reader data

Curves from different repeats were averaged and the standard deviation estimated. Experiments carried out on different days can have slightly different lag times due to small differences in preparation times. To make the results

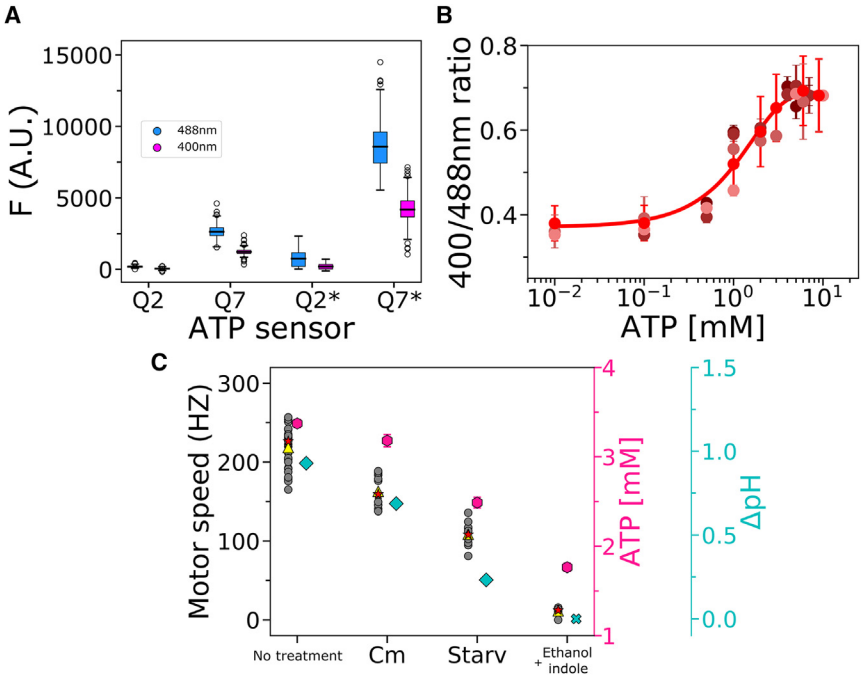

FIGURE 3 QUEEN 7μM* shows improved signal intensity and can sense in *E. coli*'s physiological range. (*A*) Comparison of the signal intensity from the four sensors. Fluorescence values for the two wavelengths of interest for the QUEEN sensor (400 and 488 nm) were obtained from 270 single cells expressing pWR20-Q2, 259 expressing pWR20-Q7, 194 expressing pWR20-Q2*, and 315 expressing pWR20-Q7*. All cells were imaged in a tunnel slide (designed as given in (39)), with the same exposure time and gain (see materials and methods). The boxplot shows lower and upper quartile and median value, with the whiskers indicating lowest and highest extremes. (*B*) Calibration curve of the Q7* sensor at 37°C and pH 7.7. Each data point is the average of three or more replicates, and the error bars show the standard deviation. Different shades of red indicate five independent experiments (each performed in replicates). Data from experiments performed on different days were rescaled as explained in the materials and methods section. The fit (*red line*) to all of the data points is used for determining ATP concentration in (*C*). (*C*) ATP and Δ pH of cells in different dormancies measured with QUEEN 7μM* sensor. The axes (*pink for ATP and* Δ *cyan for pH*) act as a legend. Measurements were made after 30 (no treatment and chloramphenicol) and 10 min (carbon starvation and indole + ethanol) from the beginning of the treatment. Gray circles indicate individual motor speeds under different conditions (median of 5-s-long recording for each cell). Total of 20, 11, 10, and 10 cells for untreated, chloramphenicol-treated, carbon-starved, and indole + ethanol-treated cells, respectively, are given. Red stars indicate the mean and yellow triangles the median values. The cytoplasmic pH values used to calculate Δ pH (cyan) are from the experiments in Fig. 2 *A* and are calculated as the mean of the pH values of all cells at the chosen time point. Where visible, the error bars indicate the standard error. Because indole interacts with our pH sensor (41), we could not measure it, but we assumed Δ pH of cells treated with indole is zero because indole is a protonophore (27). We indicate this value with a cyan cross. ATP concentration (*pink*) was measured in 493 chloramphenicol-treated and 633 carbon-starved cells. For untreated cells, we measured [ATP] of 1176, and for indole + ethanol-treated cells, 793 individual cells. The error bars show the standard error. The margin of error for our sample size and 95% confidence is 0.14 mM (5%) ATP or lower. To see this figure in color, go online.

better visible, we omitted lag periods where these were slightly longer but did not align the data in any other way.

Spectroscopy

The intensity of the light source of the SPEX Fluoromax 3 spectrometer (Horiba, JP) across the range of excitation wavelength examined was measured during data acquisition and each fluorescence measurement obtained normalized by it, thus eliminating differences due to the light source. The results of the experiments, which were carried out in triplicate, were averaged and the standard deviation calculated. The spectra obtained were normalized by the average of the replicates' values at 435-nm excitation, which is the isosbestic point of the QUEEN spectrum, insensitive to ATP concentration.

RESULTS

Carbon starvation and bacteriostatic drugs can induce instantaneous dormancy of a large population of cells

To investigate the energetics of bacterial dormancy, we focused on *E. coli* and started by establishing a working definition of dormancy based on its most widely accepted hallmarks: growth arrest and viability. We note that this is one requirement less than (46), where in addition to being viable and nongrowing, dormant cells also did not produce a reporter protein (interpreted as absence of protein production as a whole). We have chosen to relax this requirement as even cells that have been starved for long periods (more than 2 days) are now known to maintain a certain level of translation (47). Rather than focusing on dormant cells that stochastically emerge in low numbers in a heterogeneous population, we sought to induce dormancy uniformly in the entire cell population using environmental cues. This not only enables the characterization of the specific effects of a large variety of environmental cues, but it also unlocks the possibility of deploying assays, such as those necessary for PMF estimation, which are low in throughput but high in precision and time resolution. Because we wanted the measurements to be representative of the whole cell population, we minimized heterogeneity within the population before its entrance into dormancy by growing the cultures to balanced growth. Specifically, we allowed the cells to grow for $\sim$ 15 generations in exponential growth (48,49), ensuring that any cellular contents that may have been carried on from the lag phase were negligible. We also ensured that all of the experimental steps

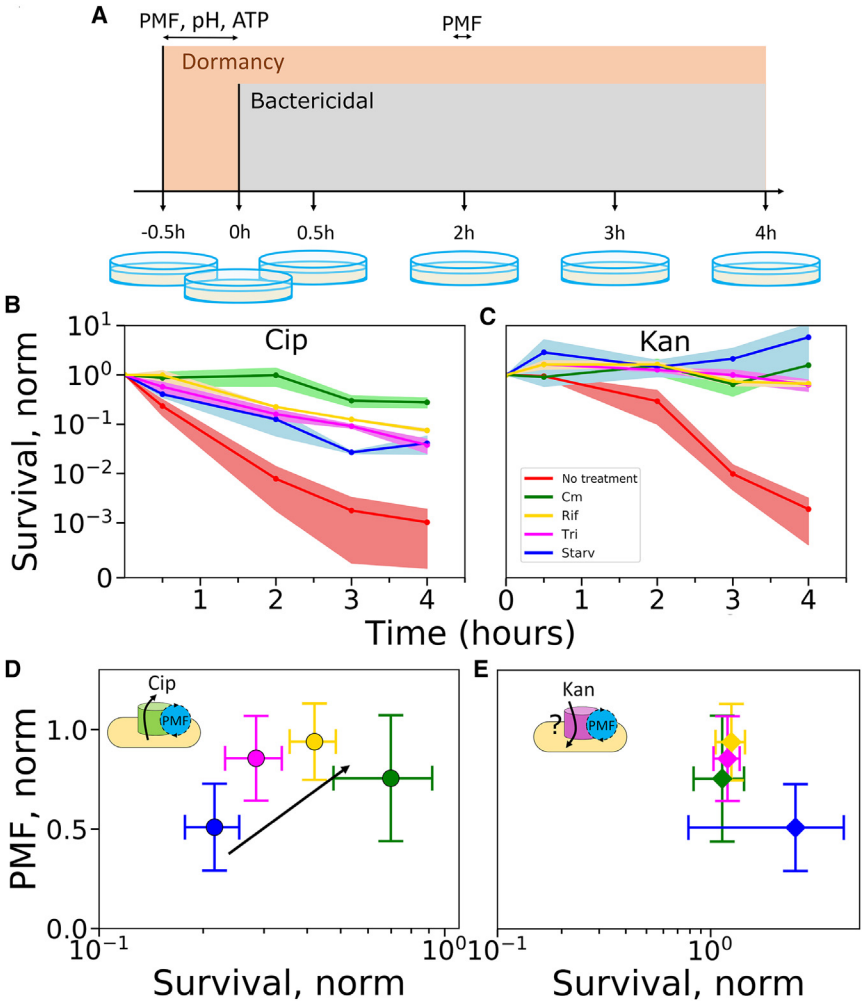

FIGURE 4 Dormant cells' survival to antibiotic treatment (at 5x MIC). (*A*) Cartoon showing the time points at which dormancy is induced and bactericidal antibiotics are added (*orange and gray*), as well as time points at which survival is estimated (*petri dishes*) and at which energetics are measured. The bactericidal antibiotics were added 30 min from initiation of dormancy, and CFUs were counted 30, 120, 180, and 240 min after the addition of the bactericidal antibiotics. (*B*) Survival to treatment with ciprofloxacin and (*C*) kanamycin. Cells that have gone dormant as a consequence of chloramphenicol, rifampicin, trimethoprim treatment, or carbon starvation are shown in green, yellow, fuchsia, and blue, respectively. These are compared with a positive control in which cells are not dormant. CFU counts are normalized by the value right before the bactericidal antibiotic addition, i.e., 30 min after initiation of dormancy. Solid lines show the median of three independent replicates and shaded areas the standard error of the mean. (*D* and *E*) Survival to antibiotic treatment plotted against normalized PMF levels of dormant cells before the treatment. Error bars show the standard deviation. Survival is estimated as the total area under the curves in (*B*), and (*C*), normalized to the CFU value right before addition of bactericidal antibiotic and divided by the total time (4 h). The PMF is taken as the average of the last minute of the bacterial flagellar motor traces in Fig. 2 *C* (after 29, 29, 29, and 9 min from the beginning of treatment for chloramphenicol, rifampicin, trimethoprim, and starvation, respectively) and normalized to the average of the first minute. To see this figure in color, go online.

were carried out at 37°C. To start, we tested six different conditions that bacteria can encounter during infection and that could cause dormancy: 1) carbon starvation, 2) nitrogen starvation, 3) indole presence (a putative quorum sensing molecule produced by stationary phase cultures that has been shown to act as a protonophore (27,50,51)), 4) chloramphenicol treatment (bacteriostatic antibiotic that stops protein synthesis (52)), 5) rifampicin treatment (bacteriostatic antibiotic blocking RNA synthesis (53)) and 6) trimethoprim treatment (bacteriostatic antibiotic that halts DNA synthesis (54)). We assayed whether these arrest growth immediately upon being presented to the cells and evaluated posttreatment viability. To assess growth arrest, we grew the cells in balanced growth as described above and then either moved them to the same growth medium but with no carbon or nitrogen or exposed them to different concentrations of the bacteriostatic drugs or indole in the same medium (Figs. 1 *A* and S1). To estimate growth, we monitored bacterial cell numbers over time via OD in a plate reader. Fig. 1 *A* shows that, as pinpointed by the characterization we report in Fig. S1, carbon starvation, 200 μg/mL chloramphenicol, 16 μg/ml rifampicin, and 0.2 μg/ml trimethoprim cause immediate growth arrest with the OD remaining constant. However, OD is an indirect measure of cell number, with a proportionality that is linear only as long as cell size and index of refraction remain constant (55). Thus, we checked that our candidate dormancies were not causing significant cell size changes by monitoring the cells in a microscope. Via microscopy, we also confirmed that constant OD was not a result of matching growth and lysis rate. Removing just the nitrogen source did not cause growth arrest, perhaps, and as pinpointed by others before (56), because traces of ammonium are often found in various chemicals and can, at least to some extents, support bacterial growth (Fig. S1 *A*). Treatment with indole stopped cell growth at a concentration of 10 mM (Fig. S1 *B*). Next, we tested cells' viability under our candidate dormancies by withdrawing aliquots from the cultures after 30, 60, 120, 180, and 240 min of treatment, washing them into fresh media, and counting the CFUs (Fig. 1 *B*). We found that chloramphenicol decreased viability to half over the 4 h, whereas carbon starvation rifampicin and trimethoprim

treatment had no effect on cell viability. Lastly, indole did not satisfy our definition of dormancy because at 10 mM, it was lethal to 99.7% of the cells (Fig. S1 *F*) (smaller concentrations of indole did not arrest growth). Our findings are consistent with a previous study that sought to induce a large number of persisters in a population with rifampicin and chloramphenicol treatment (57).

The PMF of dormant cells varies in a condition-dependent manner

Having individuated dormancies that satisfied our definition, and having obtained whole dormant populations, we investigated their energy levels by simultaneously measuring single-cell PMF and one of its two components, Δ pH, across the plasma membrane. We used the assays we previously developed (27,34,41). Briefly, bacterial flagellar motor speed is a proxy for relative PMF changes because it varies linearly with PMF (26,58). To measure the motor speed, we attached bacterial cells to the surface of a glass coverslip and polystyrene beads to genetically modified, truncated flagellar filaments (27,39,41,59). We measured the bead position, now rotated by the motor, with back focal plane interferometry, gaining information on motor speed (27,39). We carried out the measurements continuously throughout the treatment to include the transition into dormancy as well as the energy levels during dormancy. The method allows us to measure the PMF of one cell per experiment (the one placed in the heavily attenuated optical trap). To simultaneously measure Δ pH, we expressed pHluorin, a ratiometric, pH-sensitive fluorescent protein in the cell cytoplasm, and read its ratiometric signal every 90 s. We did so for the cell in which we were simultaneously measuring the PMF but also on all other neighboring cells in the same field of view (Fig. 2 *A*). The illumination conditions we used had been characterized previously and resulted in negligible photobleaching and caused no damage to *E. coli* (27). Fig. S2 shows the calibration curve we used to convert ratiometric measurements to pH (41). The experiments were carried out in a flow cell we designed (34), which allowed the transition into dormancy and continuous perfusion of our cells with fresh medium of a known pH. Like before, we performed our measurements on cultures that had grown for ∼ 15 generations in fresh medium (Fig. S3), therefore reaching balanced exponential growth with a doubling time of 57 min before the transition into dormancy. Fig. 2 shows the characteristic energy profiles of different dormancies. In particular, cells treated with chloramphenicol lost ∼ 25% of their PMF over the first 20 min of treatment settling onto this baseline thereafter (Fig. 2 *D*, green trace). Cells treated with rifampicin did not lose PMF over the first 30 min, but after ∼ 2 h, the PMF was ∼ 30% lower. Cells treated with trimethoprim gradually lost ∼ 15% of their PMF over 30 min, and we could not find any spinners after 2 h treatment. We could not establish whether this was due to full loss of PMF or whether the drug could have any effects on the assembly of motors. Cells experiencing carbon starvation settled onto a new, ∼ 50% lower PMF baseline within 2–3 min (Fig. 2 *D*, blue trace). In all cases but in the presence of rifampicin, internal pH (Fig. 2 *B*) decreased as well. By the end of the period, we measured (10 or 30 min), it dropped by Δ pH 0.15, 0.05, and 0.6 for chloramphenicol, trimethoprim, and carbon starvation, respectively. We note that the first two pH values measured in all but the control cells appear slightly higher, corresponding to the period cells are kept in the microscope slide with no flow (∼ 10 min needed to prepare the experiment and before the flow initiates the treatment, i.e., dormancy).

QUEEN* is an improved QUEEN-based ATP sensor

Having measured PMF levels during dormancy, we next focused on the ATP concentrations. Because, like we did for pH, we wished to measure time courses simultaneously with single-cell PMF measurements, we chose the QUEEN ATP sensor (42). However, the sensor suffers from poor signal intensity and requires exposure times of 1–2 s at short wavelengths, which can quickly lead to cell damage (27,34). Therefore, we focused first on optimizing the sensor's expression level and signal/noise ratio. To improve the expression level, we placed the sensor (QUEEN 2mM and QUEEN 7μM (42)) downstream of the strong constitutive promoter of the cytochrome C oxidase from *V. Harveij* (35). We also removed the histidine sequence with which the QUEEN sensors had been tagged in (42) for protein purification finding that, particularly for QUEEN 7μM, the removal of the tag produced an increase in signal intensity (Figs. 3 *A* and S4 *A*). We named these brighter derivatives QUEEN 2mM* (Q2*) and QUEEN 7μM* (Q7*). Because in (42) the His-tag is positioned in the proximity of the ATP sensing region, we reasoned that its removal could have an effect on the protein's response to ATP (especially because in vivo ATP is commonly found in coordination with magnesium ions (60)). We characterized our brightest new sensor (Q7*) in vitro working with cells' lysates (see materials and methods). The removal of the His-tag did not change spectral properties of the protein (Fig. S4 *B*), but the sensitivity range shifted toward higher [ATP] (Fig. 3 *B*), making Q7* suitable for performing ATP measurements in the physiological range of *E. coli* (42). We also found that the sensor exhibits a slight temperature dependence, shifting the sensitivity range toward higher [ATP] at 37°C compared with room temperature (Fig. S4 *E*). The calibration should, therefore, be performed for the specific temperatures at which the experiments are carried out. We next tested the pH sensitivity of Q7* and found that the sensitivity of the sensor to [ATP] changes little in the pH 7.2 to 7.6 range. For pH above 7.8, the fluorescence

ratio (of the 400/488 nm) decreases for the same [ATP], and it is overall significantly less sensitive to [ATP] changes. Next, we assessed the sensor's photostability, first focusing on whether photobleaching altered ATP calibration (Fig. S5). Again, using cell lysates for the in vitro characterization, we observed that both the 400 and 488 nm wavelengths can photobleach (Fig. S5 *A–C*). We also characterized the sensor's photostability inside the cells. Because short wavelength illumination can lead to significant photodamage (27), we characterized it first by monitoring bacterial PMF under different illumination frame rates. We found that when illuminated every 7 min with 488 and 400 nm wavelengths for 20 min total, cells experience no photodamage (Fig. S5 *D–F*). We then sought to decouple the behavior of the QUEEN sensor from cellular physiology by treating bacteria with 5% ethanol, which drops the PMF (27) and presumably limits any physiologically driven changes in the intracellular [ATP]. After 15 min, and still keeping the ethanol in, we exposed the cells to illumination at different frame rates. As expected, we observed exposure-dependent photobleaching at the 400 nm wavelength (Fig. S5 *G*). Contrary to our observations with lysates, the signal from the 488 nm wavelength showed a time-dependent intensity increase (Fig. S5 *H*), where the 400/488 ratio decreased significantly with illumination (Fig. S5 *I*). The time-dependent increase in intensity under 488-nm illumination could be explained by photoactivation, a light-dependent red shift common among GFP and its derivatives (61,62), or by a drop in the [ATP]. As the cells have been pretreated with ethanol, we deemed the latter less likely, but we further confirmed it by exposing cells to even stronger concentrations of PMF decouplers: a mixture of 2% ethanol and 10 mM indole, which acts as a protonophore and immediately shuts down most of the PMF (Fig. S6 *C*) (27,50,51). As shown in Fig. S6, the protein in these cells shows similar behavior to that in Fig. S5. We concluded that the increase in intensity observed under 488-nm illumination was most likely caused by photoactivation and that, given the sensor's photo properties, time series measurements should be replaced with an estimate of cellular [ATP] at only one time point.

PMF, cytoplasmic pH, and ATP concentration are coupled during dormancy

Having characterized the ATP sensor, we set out to measure PMF, cytoplasmic pH, and ATP concentration in dormant cells. Because our pH and ATP sensors share similar spectral properties, pH and ATP measurements could not be performed in the same cells. Instead, we carried out [ATP] measurements while simultaneously monitoring flagellar motor speed, in a similar fashion to Fig. 2 (where we simultaneously monitored PMF and pH). As a time point for ATP estimation, and while PMF was being monitored, we chose 10 min after initiation of dormancy for carbon-starved cells and 30 min for chloramphenicol-treated cells. We did not measure [ATP] in the other two bacteriostatic drugs, because these only caused small PMF changes in the 30-min interval. We also measured [ATP] in the cells before any treatment, as well as in cells treated with the 2% ethanol + 10 mM indole mixture (after 10 min of treatment). The latter rapidly collapses most of the PMF. The trends of PMF upon treatment for strains expressing the Q7* ATP sensor recapitulated the ones we observed in Figs. 2 and 3 *C* show the ATP levels of the two dormancies. Cells treated with a bacteriostatic antibiotic maintain seemingly constant ATP levels, despite losing $\sim$ 25% of their PMF, whereas cells deprived of carbon that lost $\sim$ 50% loss of PMF quickly lose one-third of their ATP. As expected, cells treated with the ethanol and indole mixture show the most marked ATP loss, and overall the observed [ATP] is within the same order of magnitude as previously reported by (42). The [ATP] measurements were done at the following cytoplasmic pHs: 8.1 for the positive control, 7.9 for chloramphenicol, 7.4 for carbon starvation, and 7.2 for the negative control. At pHs above 7.8, the 400/488 nm ratio of the Q7* sensor decreases (Fig. S4 *E*), so the ATP values for untreated and antibiotic-treated cells may be underestimated. However, they still confirm the overall trend of cellular energetics, where loss of PMF results in loss of ATP, albeit possibly not to the same relative extent.

Dormant states with different energy levels show various degrees of susceptibility to antibiotics of different classes

Having established that different dormancies have different energetic profiles, we wondered if these influenced antibiotic susceptibility. Previous findings show that cellular energy levels play a role in antibiotic efficacy, e.g., by governing aminoglycoside drugs uptake rate (63), fueling multidrug efflux pumps activity (32), or other cellular response mechanisms such as DNA repair (64,65). We exposed exponentially growing cells to the four dormancies, as in Fig. 2. After 30 min, when cells were dormant, we exposed the cultures to 5x MIC concentration of two bactericidal drugs, ciprofloxacin and kanamycin. The former is a DNA-damaging drug thought to be a substrate of multidrug efflux pumps (66,67), and kanamycin is an aminoglycoside that causes errors in protein translation (68). Aminoglycoside uptake is PMF dependent (although under certain conditions PMF-independent uptake has been identified as well (69)) and proceeds in phases (63,70,71). Cells were kept in dormancy-inducing conditions during the treatment with bactericidal drugs. The MIC concentrations were obtained as explained in materials and methods and shown in Fig. S7. We assayed survival of dormant cells under ciprofloxacin and kanamycin treatment for up to 4 h, by withdrawing aliquots at regular intervals and performing CFU counting. Fig. 4 *A* illustrates our experimental protocol. For all dormancies tested, dormant cells cope significantly

better than growing cells (our positive control), confirming the protective role of dormancy (Fig. 4 *B* and *C*). All of the dormancies we selected offered complete protection from kanamycin treatment (Fig. 4 *B* and *C*), whereas for ciprofloxacin, we observed dormancy-specific differences (Fig. 4 *D*). In its presence, carbon-starved cells died faster than cells treated with bacteriostatic antibiotics, with only three cells in 100 remaining alive after 3 h of treatment. Chloramphenicol-treated cells died the slowest; even after 4 h, more than a fourth of the population was still alive. Because ciprofloxacin is a known substrate of PMF-dependent efflux pumps, our results could be coherent with an energy-dependent drug accumulation model, whereby highly energetic dormant cells survive because they can better use energy-fueled efflux pumps to export the antibiotic (Fig 4 *D*). On the other hand, scarcely energetic dormant cells should deal better with antibiotics whose active import in the cell is energy dependent, like kanamycin. However, in our dormant states and kanamycin concentrations tested, all cells survived the drug, suggesting that energetics do not play a substantial role in protecting the cells from kanamycin during dormancy.

DISCUSSION

Many antibiotics interfere with molecular targets that are essential during cell growth. Dormancy is thought to protect bacteria by making these drug targets nonessential. Yet the picture is probably more complex as not all nongrowing cells are equally protected from antibiotics (46), and the mechanisms behind these differences remain an open question. In this work, we deployed an ATP concentration sensor, a cytoplasmic pH sensor, and an assay for PMF measurements to investigate the physiology of dormant cells at the single-cell level. Rather than using an approach in which dormancy, and thus drug survival, emerge stochastically at a low frequency, we chose to induce dormancy a priori. This had several advantages. First, it allowed us to bypass the use of high-persistent genetic backgrounds, like *hipA7*, and allowed us to work in an effectively wild-type background. Second, it gave us the freedom of testing various controlled conditions that can potentially occur at the infection site and directly link them to their effects on cells' phenotype. Third, because the whole cell population is exposed to dormancy-inducing conditions, we could carry out low yield but highly informative assays such as flagellar motor speed measurements, yet obtain sufficient sample size. Our results show that cells that have gone dormant due to different external conditions settle onto markedly different energy profiles. In particular, across the conditions tested, energy levels range from growth-like to significantly reduced, indicating that the dormant state is much richer in phenotypical diversity than previously thought.

Looking at susceptibility to different antibiotics, we confirm that dormant cells outperform growing ones in terms of survival. Additionally, we presented evidence that for the aminoglycoside kanamycin growth arrest produces an almost complete protection, whereas survival to the fluoroquinolone ciprofloxacin correlates with the PMF levels of each dormancy. Based on this correlation, we can speculate that the energy profile during dormancy could be an important factor in the survival to ciprofloxacin. This is not only in agreement with previous work showing that stationary phase cells are susceptible to the drug (72), but it is also coherent with reports indicating that the main mechanisms of survival to ciprofloxacin involve drug efflux pumps and the SOS response (73), both energy-costly processes (74,75). In the case of kanamycin, the protection caused by growth arrest seems to mask any energy-dependent effects in our conditions, suggesting that PMF-dependent uptake of aminoglycosides previously reported is not a sufficiently costly process at the maintenance energy levels we here observed. It is not excluded that more prominent trends might emerge at higher drug concentrations or in dormant conditions that are less energetic than the carbon starvation we tested.

Taken together, our results pave the way for a typologization of dormancy based on the association between its causative factors and the cells' physiological parameters. We show that the different dormancy types are physiologically and clinically relevant, as we demonstrate correlations between environmental conditions and drug susceptibility of dormant cells. These results offer a mechanistic explanation for the different and seemingly contradictory antibiotic efficacies observed by others who have attempted to establish a general link among dormancy, energetics, and treatment outcomes. Furthermore, our data showing that in some cases high energy can reduce antibiotic efficacy suggest that treatments based on the awakening of dormant cells by boosting metabolism may in some cases be counterproductive. Although our evidence was obtained on cell populations that have been made dormant en masse, we expect our conclusions to be relevant for variations in energy levels that emerge stochastically across cell populations, and we speculate that our results could be informative for dormancy and dormancy-like phenomena in other organisms.

Because antibiotics are just one example of the stressors bacteria are capable of withstanding through dormancy, a typologization of nongrowing states is much needed not only from the point of view of treatment but also to understand how microbes survive and evolve in the environment, where periods of growth interruption or limitation are the norm. The energetic makeup is likely to play a primary role in the maintenance of viability in these settings and by determining which cells are able to repair their DNA, express newly acquired genes (76), and replicate their genomes, may be a driver of evolution.

DATA AVAILABILITY

All data is deposited at https://doi.org/10.7488/ds/7476.

SUPPORTING MATERIAL

Supporting material can be found online at https://doi.org/10.1016/j.bpj.2023.06.023.

AUTHOR CONTRIBUTIONS

L.M. and T.P. conceived the experiments. L.M. performed the experiments and analyzed experimental data. L.M. and T.P. interpreted the results and wrote the manuscript.

ACKNOWLEDGMENTS

We are grateful to Hideyuki Yaginuma for donating constructs containing the QUEEN sensors and for providing us the published data with QUEEN excitation spectrum. We are also grateful to Alessia Lepore and Meriem El Karoui for donating an aliquot of ciprofloxacin and to members of Pilizota lab as well as Alessia Lepore, Meriem El Karoui, Ssu-Yuan Lin, Chien-Jung Lo, and Thomas Julou for useful discussions. We are grateful to Pietro Cicuta for advice and support during the preparation of the manuscript.

This work was financially supported by the Cunningham Trust scholarship ACC/KWF/PhD1 to T.P. and L.M. T.P. acknowledges the support of Human Frontier Science Program Grant (RGP0041/2015) and UK Research Councils Synthetic Biology for Growth program and is a member of the Biotechnology and Biological Sciences Research Council and Physical Sciences Research Council/Medical Research Council-funded Synthetic Biology Research Centre (BB/M018040/1).

DECLARATION OF INTERESTS

The authors declare no competing interests.

REFERENCES

1. Murray, C. J., K. S. Ikuta, …, M. Naghavi. 2022. Global burden of bacterial antimicrobial resistance in 2019: A systematic analysis. *Lancet.* 399:629–655.
2. Brauner, A., O. Fridman, …, N. Q. Balaban. 2016. Distinguishing between resistance, tolerance and persistence to antibiotic treatment. *Nat. Rev. Microbiol.* 14:320.
3. Balaban, N. Q., S. Helaine, …, A. Zinkernagel. 2019. Definitions and guidelines for research on antibiotic persistence. *Nat. Rev. Microbiol.* 17:441–448.
4. Lewis, K. 2007. Persister cells, dormancy and infectious disease. *Nat. Rev. Microbiol.* 5:48–56.
5. Grant, S. S., and D. T. Hung. 2013. Persistent bacterial infections, antibiotic tolerance, and the oxidative stress response. *Virulence.* 4:273–283.
6. Levin-Reisman, I., I. Ronin, …, N. Q. Balaban. 2017. Antibiotic tolerance facilitates the evolution of resistance. *Science.* 355:826–830.
7. Liu, J., O. Gefen, …, N. Q. Balaban. 2020. Effect of tolerance on the evolution of antibiotic resistance under drug combinations. *Science.* 367:200–204.
8. Sebastian, J., S. Swaminath, …, P. Ajitkumar. 2017. De novo emergence of genetically resistant mutants of mycobacterium tuberculosis from the persistence phase cells formed against antituberculosis drugs in vitro. *Antimicrob. Agents Chemother.* 61, e01343-16.
9. Windels, E. M., J. E. Michiels, …, J. Michiels. 2019. Bacterial persistence promotes the evolution of antibiotic resistance by increasing survival and mutation rates. *ISME J.* 13:1239–1251.
10. Rittershaus, E. S. C., S.-H. Baek, and C. M. Sassetti. 2013. The normalcy of dormancy: Common themes in microbial quiescence. *Cell Host Microbe.* 13:643–651.
11. Ronneau, S., and S. Helaine. 2019. Clarifying the link between toxin–antitoxin modules and bacterial persistence. *J. Mol. Biol.* 431:3462–3471, The molecular basis of antibiotic action and resistance.
12. Shan, Y., A. Brown Gandt, …, K. Lewis. 2017. Atp-dependent persister formation in *Escherichia coli*. *mBio.* 8.
13. Conlon, B. P., S. E. Rowe, …, K. Lewis. 2016. Persister formation in staphylococcus aureus is associated with atp depletion. *Nat. Microbiol.* 1, 16051.
14. Braetz, S., P. Schwerk, …, M. Fulde. 2017. The role of atp pools in persister cell formation in (fluoro)quinolone-susceptible and -resistant strains of salmonella enterica ser. typhimurium. *Vet. Microbiol.* 210:116–123.
15. D. Leszczynska, E. Matuszewska, …, E. Laskowska, "The formation of persister cells in stationary-phase cultures of *Escherichia coli* is associated with the aggregation of endogenous proteins," PLoS One, vol. 8, pp. e54737–54810, 01 2013.
16. Svenningsen, M. S., A. Veress, …, S. Semsey. 2019. Birth and resuscitation of (p)ppgpp induced antibiotic tolerant persister cells. *Sci. Rep.* 9:6056.
17. Aedo, S. J., M. A. Orman, and M. P. Brynildsen. 2019. Stationary phase persister formation in *Escherichia coli* can be suppressed by piperacillin and pbp3 inhibition. *BMC Microbiol.* 19:140.
18. Lobritz, M. A., P. Belenky, …, J. J. Collins. 2015. Antibiotic efficacy is linked to bacterial cellular respiration. *Proc. Natl. Acad. Sci. USA.* 112:8173–8180.
19. Wilmaerts, D., M. Bayoumi, …, G. Storz. 2018. The persistence-inducing toxin hokb forms dynamic pores that cause atp leakage. *mBio.* 9:e00744-18.
20. Manuse, S., Y. Shan, …, K. Lewis. 2021. Bacterial persisters are a stochastically formed subpopulation of low-energy cells. *PLoS Biol.* 19:e3001194.
21. Pontes, M. H., and E. A. Groisman. 2019. Slow growth determines nonheritable antibiotic resistance in salmonella enterica. *Sci. Signal.* 12:eaax3938.
22. Kaldalu, N., V. Hauryliuk, and T. Tenson. 2016. Persisters—as elusive as ever. *Appl. Microbiol. Biotechnol.* 100:6545–6553.
23. Balaban, N. Q., J. Merrin, …, S. Leibler. 2004. Bacterial persistence as a phenotypic switch. *Science.* 305:1622–1625.
24. Łapińska, U., M. Voliotis, …, S. Pagliara. 2022. Fast bacterial growth reduces antibiotic accumulation and efficacy. *Elife.* 11, e74062.
25. Magariyama, Y., S. Sugiyama, …, S. Kudo. 1995. Simultaneous measurement of bacterial flagellar rotation rate and swimming speed. *Biophys. J.* 69:2154–2162.
26. Gabel, C. V., and H. C. Berg. 2003. The speed of the flagellar rotary motor of *Escherichia coli* varies linearly with protonmotive force. *Proc. Natl. Acad. Sci. USA.* 100:8748–8751.
27. Krasnopeeva, E., C.-J. Lo, and T. Pilizota. 2019. Single-cell bacterial electrophysiology reveals mechanisms of stress-induced damage. *Biophys. J.* 116:2390–2399.
28. Jahreis, K., E. F. Pimentel-Schmitt, …, F. Titgemeyer. 2008. Ins and outs of glucose transport systems in eubacteria. *FEMS Microbiol. Rev.* 32:891–907.
29. Wood, J. M. 2015. Bacterial responses to osmotic challenges. *J. Gen. Physiol.* 145:381–388.
30. Ramos, S., and H. R. Kaback. 1977. The relation between the electrochemical proton gradient and active transport in *Escherichia coli* membrane vesicles. *Biochemistry.* 16:854–859.
31. Bradbeer, C. 1993. The proton motive force drives the outer membrane transport of cobalamin in *Escherichia coli*. *J. Bacteriol.* 175:3146–3150.
32. Anes, J., M. P. McCusker, …, M. Martins. 2015. The ins and outs of rnd efflux pumps in *Escherichia coli*. *Front. Microbiol.* 6:587.

33. Terradot, G., E. Krasnopeeva, …, T. Pilizota. 2021. The proton motive force determines *Escherichia coli*'s robustness to extracellular Ph. Preprint at bioRxiv. https://doi.org/10.1101/2021.11.19.469321.
34. Mancini, L., G. Terradot, …, T. Pilizota. 2020. A general workflow for characterization of nernstian dyes and their effects on bacterial physiology. *Biophys. J.* 118:4–14.
35. Pilizota, T., and J. W. Shaevitz. 2012. Fast, multiphase volume adaptation to hyperosmotic shock by *Escherichia coli*. *PLoS One.* 7, e35205.
36. Neidhardt, F. C., P. L. Bloch, and D. F. Smith. 1974. Culture medium for enterobacteria. *J. Bacteriol.* 119:736–747.
37. University Of Wisconsin (USA). 2020. Rich Defined Medium Protocol. https://www.genome.wisc.edu/resources/protocols/ezmedium.htm.
38. Brouwers, R., H. Vass, …, R. J. Allen. 2020. Stability of β-lactam antibiotics in bacterial growth media. *PLoS One.* 15:e0236198.
39. Rosko, J., V. A. Martinez, …, T. Pilizota. 2017. Osmotaxis in *Escherichia coli* through changes in motor speed. *Proc. Natl. Acad. Sci. USA.* 114:E7969–E7976.
40. Krasnopeeva, E. 2018. Single cell measurements of bacterial physiology traits during exposure to an external stress. *In* PhD Thesis University of Edinburgh.
41. Wang, Y.-K., E. Krasnopeeva, …, C.-J. Lo. 2019. Comparison of *Escherichia coli* surface attachment methods for single-cell microscopy. *Sci. Rep.* 9, 19418.
42. Yaginuma, H., S. Kawai, …, H. Imamura. 2014. Diversity in atp concentrations in a single bacterial cell population revealed by quantitative single-cell imaging. *Sci. Rep.* 4:6522.
43. Jett, B. D., K. L. Hatter, …, M. S. Gilmore. 1997. Simplified agar plate method for quantifying viable bacteria. *Biotechniques.* 23:648–650.
44. Schneider, C. A., W. S. Rasband, and K. W. Eliceiri. 2012. Nih image to imagej: 25 years of image analysis. *Nat. Methods.* 9:671–675.
45. Otsu, N. 1979. A threshold selection method from gray-level histograms. *IEEE Trans. Syst. Man Cybern.* 9:62–66.
46. Gefen, O., C. Gabay, …, N. Q. Balaban. 2008. Single-cell protein induction dynamics reveals a period of vulnerability to antibiotics in persister bacteria. *Proc. Natl. Acad. Sci. USA.* 105:6145–6149.
47. Bergkessel, M., and L. Delavaine. 2021. Diversity in starvation survival strategies and outcomes among heterotrophic Proteobacteria. *Microb. Physiol.* 31:146–162.
48. Maaløe, O., and N. O. Kjeldgaard. 1966. Control of Macromolecular Synthesis: A Study of DNA, RNA, and Protein Synthesis in Bacteria. W.A. Benjamin..
49. Harvey, R. J., and A. L. Koch. 1980. How partially inhibitory concentrations of chloramphenicol affect the growth of *Escherichia coli*. *Antimicrob. Agents Chemother.* 18:323–337.
50. Chimerel, C., C. M. Field, …, D. K. Summers. 2012. Indole prevents *Escherichia coli* cell division by modulating membrane potential. *Biochim. Biophys. Acta.* 1818:1590–1594.
51. Kim, J., and W. Park. 2015. Indole: a signaling molecule or a mere metabolic byproduct that alters bacterial physiology at a high concentration? *J. Microbiol.* 53:421–428.
52. Gale, E. F., and J. P. Folkes. 1953. The assimilation of amino-acids by bacteria. xv. actions of antibiotics on nucleic acid and protein synthesis in staphylococcus aureus. *Biochem. J.* 53:493–498.
53. Hartmann, G., K. O. Honikel, …, J. Nüesch. 1967. The specific inhibition of the dna-directed rna synthesis by rifamycin. *Biochim. Biophys. Acta Nucleic Acids Protein Synth.* 145:843–844.
54. Brogden, R. N., A. A. Carmine, …, G. S. Avery. 1982. Trimethoprim: A review of its antibacterial activity, pharmacokinetics and therapeutic use in urinary tract infections. *Drugs.* 23:405–430.
55. Stevenson, K., A. F. McVey, …, T. Pilizota. 2016. General calibration of microbial growth in microplate readers. *Sci. Rep.* 6, 38828.
56. Kim, M., Z. Zhang, …, T. Hwa. 2012. Need-based activation of ammonium uptake in *Escherichia coli*. *Mol. Syst. Biol.* 8:616.
57. Kwan, B. W., J. A. Valenta, …, T. K. Wood. 2013. Arrested protein synthesis increases persister-like cell formation. *Antimicrob. Agents Chemother.* 57:1468–1473.
58. Fung, D. C., and H. C. Berg. 1995. Powering the Flagellar Motor of *Escherichia coli* with an External Voltage Source.
59. Ryu, W. S., R. M. Berry, and H. C. Berg. 2000. Torque-generating units of the flagellar motor of *Escherichia coli* have a high duty ratio. *Nature.* 403:444–447.
60. Gout, E., F. Rébeillé, …, R. Bligny. 2014. Interplay of mg2+, adp, and atp in the cytosol and mitochondria: Unravelling the role of mg2+ in cell respiration. *Proc. Natl. Acad. Sci. USA.* 111:E4560–E4567.
61. Elowitz, M. B., M. G. Surette, …, S. Leibler. 1997. Photoactivation turns green fluorescent protein red. *Curr. Biol.* 7:809–812.
62. Patterson, G. H., and J. Lippincott-Schwartz. 2002. A photoactivatable gfp for selective photolabeling of proteins and cells. *Science.* 297:1873–1877.
63. Taber, H. W., J. P. Mueller, …, A. S. Arrow. 1987. Bacterial uptake of aminoglycoside antibiotics. *Microbiol. Rev.* 51:439–457.
64. Kowalczykowski, S. C. 1991. Biochemistry of genetic recombination: energetics and mechanism of dna strand exchange. *Annu. Rev. Biophys. Biophys. Chem.* 20:539–575.
65. Kowalczykowski, S. C., D. A. Dixon, …, W. M. Rehrauer. 1994. Biochemistry of homologous recombination in *Escherichia coli*. *Microbiol. Rev.* 58:401–465.
66. Giraud, E., A. Cloeckaert, …, E. Chaslus-Dancla. 2000. Evidence for active efflux as the primary mechanism of resistance to ciprofloxacin in *salmonella enterica* serovar typhimurium. *Antimicrob. Agents Chemother.* 44:1223–1228.
67. Piddock, L. J. V. 2006. Clinically relevant chromosomally encoded multidrug resistance efflux pumps in bacteria. *Clin. Microbiol. Rev.* 19:382–402.
68. Jelenc, P. C., and C. G. Kurland. 1984. Multiple effects of kanamycin on translational accuracy. *Mol. Gen. Genet.* 194:195–199.
69. Radlinski, L. C., S. E. Rowe, …, B. P. Conlon. 2019. Chemical induction of aminoglycoside uptake overcomes antibiotic tolerance and resistance in staphylococcus aureus. *Cell Chem. Biol.* 26:1355–1364.e4.
70. Krause, K. M., A. W. Serio, …, L. E. Connolly. 2016. Aminoglycosides: An overview. *Cold Spring Harb. Perspect. Med.* 6:a027029.
71. Ramirez, M. S., and M. E. Tolmasky. 2010. Aminoglycoside modifying enzymes. *Drug Resist. Updates.* 13:151–171.
72. Zeiler, H. J. 1985. Evaluation of the in vitro bactericidal action of ciprofloxacin on cells of *Escherichia coli* in the logarithmic and stationary phases of growth. *Antimicrob. Agents Chemother.* 28:524–527.
73. Tran, T., Q. Ran, …, A. Khodursky. 2016. De novo characterization of genes that contribute to high-level ciprofloxacin resistance in *Escherichia coli*. *Antimicrob. Agents Chemother.* 60:6353–6355.
74. Blanco, P., S. Hernando-Amado, …, J. L. Martinez. 2016. Bacterial multidrug efflux pumps: Much more than antibiotic resistance determinants. *Microorganisms.* 4, 14.
75. Händel, N., J. M. Schuurmans, …, B. H. ter Kuile. 2013. Compensation of the metabolic costs of antibiotic resistance by physiological adaptation in *Escherichia coli*. *Antimicrob. Agents Chemother.* 57:3752–3762.
76. Kolter, R., N. Balaban, and T. Julou. 2022. Bacteria grow swiftly and live thriftily. *Curr. Biol.* 32:R599–R605.